1524 *Inorg. Chem.* **2010**, *49*, 1524–1534
DOI: 10.1021/ic901903f

Inorganic Chemistry
Article

Anomalous Non-Prussian Blue Structures and Magnetic Ordering of $K_2Mn^{II}[Mn^{II}(CN)_6]$ and $Rb_2Mn^{II}[Mn^{II}(CN)_6]$

Jae-Hyuk Her,[‡,§] Peter W. Stephens,*[,‡] Christopher M. Kareis,[†] Joshua G. Moore,[†] Kil Sik Min,[†,∥] Jong-Won Park,[†] Garima Bali,[†] Bretni S. Kennon,[†] and Joel S. Miller*[,†]

[†]*Department of Chemistry, 315 S. 1400 E. RM 2124, University of Utah, Salt Lake City, Utah 84112-0850 and* [‡]*Department of Physics & Astronomy, Stony Brook University, Stony Brook, New York 11794-3800.* [§]*Current address: GE Global Research, 1 Research Circle, Niskayuna, NY 12309.* [∥]*Current address: Department of Chemistry Education, Kyungpook National University, Daegu, South Korea.*

Received September 29, 2009

The reaction of Mn^{II} and KCN in aqueous and non-aqueous media leads to the isolation of three-dimensional (3-D) Prussian blue analogues, $K_2Mn[Mn(CN)_6]$ (**1a**−**d**, **1e**, respectively). Use of RbCN forms $Rb_2Mn[Mn(CN)_6]$ (**2**). **1** and **2** are isomorphic {monoclinic, $P2_1/n$: **1** [a = 10.1786(1) Å, b = 7.4124(1) Å, c = 6.9758(1) Å, β = 90.206(1)°]; **2** [a = 10.4101(1) Å, b = 7.4492(1) Å, c = 7.2132(1) Å, β = 90.072(1)°]}, with a small monoclinic distortion from the face centered cubic (fcc) structure that is typical of Prussian blue structured materials that was previously reported for $K_2Mn[Mn(CN)_6]$. Most notably the average Mn−N−C angles are 148.8° and 153.3° for **1** and **2**, respectively, which are significantly reduced from linearity. This is attributed to the ionic nature of high spin Mn^{II} accommodating a reduced M−CN−M′ angle and minimizing void space. Compounds **1a,b** have a sharp, strong ν_{OH} band at 3628 cm^{-1}, while **1e** lacks a ν_{OH} absorption. The ν_{OH} absorption in **1a,b** is attributed to surface water, as use of D_2O shifts the ν_{OH} absorption to 2677 cm^{-1}, and that **1a**−**e** are isostructural. Also, fcc Prussian blue-structured $Cs_2Mn[Mn(CN)_6]$ (**3**) has been structurally [$Fm\bar{3}m$: a = 10.6061(1) Å] and magnetically characterized. The magnetic ordering temperature, T_c, increases as K^+ (41 K) > Rb^+ (34.6 K) > Cs^+ (21 K) for $A_2Mn[Mn(CN)_6]$ in accord with the increasing deviation for linearity of the Mn−N−C linkages [148.8 (K^+) > 153.3 (Rb^+) > 180° (Cs^+)], decreasing Mn(II)···Mn(II) separations [5.09 (K^+) < 5.19 (Rb^+) < 5.30 Å (Cs^+)], and decreasing size of the cation (increasing electrostatic interactions). Hence, the bent cyanide bridges play a crucial role in the superexchange mechanism by increasing the coupling via shorter Mn(II)···Mn(II) separations, and perhaps enhanced overlap. In addition, the temperature dependent magnetic behavior of $K_4[Mn^{II}(CN)_6]\cdot 3H_2O$ is reported.

Introduction

Ferri- and to a lesser extent ferromagnetic ordering has been reported for several hexacyanometalates possessing the Prussian blue structure.[1−3] Critical temperatures, T_c, as great as ∼100 °C have been reported for $KV^{II}[Cr^{III}(CN)_6]\cdot 2H_2O\cdot 0.1(KO_3SCF_3)$[3a] and $K_{0.058}V^{II}_{0.57}V^{III}_{0.43}[Cr^{III}(CN)_6]_{0.79}\cdot(SO_4)_{0.058}\cdot 0.93H_2O$[3b] with the anticipation that they may find applications in areas such as magnetic shielding[4] and spintronic memory storage devices.[5] Magnetic ordering occurs in these materials because of the strong spin coupling between adjacent metal sites via the superexchange interaction[6] of the cyanide ligand. This family includes $Mn^{III}[Mn^{III}(CN)_6]$ (T_c = 31 K),[7] $Mn^{III}_3[Mn^{II}(CN)_6]_2\cdot zH_2O$

*To whom correspondence should be addressed. E-mail: jsmiller@chem.utah.edu (J.S.M.), peter.stephens@sunysb.edu (P.W.S.).

(1) Verdaguer, M.; Girolami, G. S. In *Magnetism - Molecules to Materials*; Miller, J. S., Drillon, M., Eds.; Wiley-VCH: Weinheim, 2005, Vol. *5*, p 283. Hashimoto, K.; Ohkoshi, S. *Phil. Trans. R. Soc. Lond. A* **1999**, *357*, 2977. Verdaguer, M.; Bleuzen, A.; Marvaud, V.; Vaissermann, J.; Seuleiman, M.; Desplanches, C.; Scuiller, A.; Train, C.; Garde, R.; Gelly, G.; Lomenech, C.; Rosenman, I.; Veillet, P.; Cartier, C.; Villain, F. *Coord. Chem. Rev*. **1999**, *190*−*192*, 1023.

(2) (a) Ferlay, S.; Mallah, T.; Ouahes, R.; Veillet, P.; Verdaguer, M. *Nature* **1995**, *378*, 701. (b) Dujardin, E.; Ferlay, S.; Phan, X.; Desplanches, C.; Moulin, C. C. D.; Sainctavit, P.; Baudelet, F.; Dartyge, E.; Veillet, P.; Verdaguer, M. *J. Am. Chem. Soc*. **1998**, *120*, 11347. (c) Ferlay, S.; Mallah, T.; Ouahes, R.; Veillet, P.; Verdaguer, M. *Inorg. Chem*. **1999**, *38*, 229. (d) Verdaguer, M.; Bleuzen, A.; Train, C.; Garde, R.; Fabrizi de Biani, F.; Desplanches, C. *Phil. Trans. R. Soc. Lond. A* **1999**, *357*, 2959.

(3) (a) Holmes, S. M.; Girolami, G. S. *J. Am. Chem. Soc*. **1999**, *121*, 5593. (b) Hatlevik, Ø.; Buschmann, W. E.; Zhang, J.; Manson, J. L.; Miller, J. S. *Adv. Mater*. **1999**, *11*, 914.

(4) (a) Morin, B. G.; Hahm, C.; Epstein, A. J.; Miller, J. S. *J. Appl. Phys*. **1994**, *75*, 5782. (b) Miller, J. S. *Adv. Mater*. **1994**, *6*, 322. (c) Landee, C. P.; Melville, D.; Miller, J. S. In *NATO ARW Molecular Magnetic Materials*; Kahn, O., Gatteschi, D., Miller, J. S., Palacio, F., Eds.; Kluwer Academic Publishers: London, 1991, Vol. *E198*, p 395.

(5) Prigodin, V. N.; Raju, N. P.; Pokhodnya, K. I.; Miller, J. S.; Epstein, A. *J. Adv. Mater*. **2002**, *14*, 1230.

(6) (a) Anderson, P. W. *Phys. Rev*. **1950**, *79*, 350. (b) Goodenough, J. B. *J. Phys. Chem. Solids* **1958**, *6*, 287. (c) Kanamori, J. *J. Phys. Chem. Solids* **1959**, *10*, 87.

(7) Buschmann, W. E.; Miller, J. S. *Inorg. Chem*. **2000**, *39*, 2411.

 Published on Web 01/19/2010

($12 \leq z \leq 16$; T_c = 35.5 K),[8,9] $CsMn^{II}[Mn^{III}(CN)_6]\cdot 1/2(H_2O)$ (T_c = 31 K),[8] and $Mn^{II}[Mn^{IV}(CN)_6]\cdot 1.14H_2O$ (T_c = 49 K).[7,10] In the case of $Mn^{II}{}_3[Mn^{III}(CN)_6]_2\cdot 12H_2O$, the C-bound low spin (*ls*) Mn^{III} ($t_{2g}{}^4$, S = 1) interacts with the N-bound high spin (*hs*) Mn^{II} ($t_{2g}{}^3e_g{}^2$, S = 5/2) ferrimagnetically.[8,9] Additionally, face-centered cubic (fcc) $K_2Mn^{II}[Mn^{II}(CN)_6]$[8,11a] and $NaMn[Cr(CN)_6]$[12] were reported to be ferrimagnets with T_cs of 41 and 60 K, respectively.

Recently, $M^{II}[Mn^{IV}(CN)_6]$ (M = Co, Ni) and $M^{III}[Mn^{III}(CN)_6]$ (M = V, Cr, Mn) made in non-aqueous media showed unexpected magnetic behaviors.[7] The formation of the water-free lattice led to spin-glass behavior that is atypical of Prussian blue analogues (PBAs).[1−3] Also, the study of anhydrous $Fe[Mn(CN)_6]$ and its hydrate revealed that they have uncommon mixed valency and magnetic properties.[13]

Keggin and Miles originally reported the structure of $A_nFe[Fe(CN)_6]$ (A = alkali cation) as being fcc, and this has been recognized as the general structure for $A_nM[M'(CN)_6]\cdot zH_2O$ PBAs.[14] PBAs have two distinct metal sites consisting of C bonded to strong field metal sites, $M'C_6$, and N bonded to weak field metal sites, MN_6, and charge balancing cations and/or water molecules are located within the void spaces of each lattice. Often PBAs have incomplete lattices with water coordinated to M rather than nitrogen.[15,16]

Herein, we investigate the magnetic properties of $K_2Mn^{II}[Mn^{II}(CN)_6]$ (**1a**−**e**) and $Rb_2Mn^{II}[Mn^{II}(CN)_6]$ (**2**), and report the first non-face centered cubic structure of $A_2Mn[Mn(CN)_6]$ (A = K, Rb) composition with bent Mn−CN−Mn linkages. For comparison the magnetic behavior of $K_4[Mn^{II}(CN)_6]$ is revisited.[17] We also extend the fcc Prussian blue structure type with the preparation and structural and magnetic characterization of $Cs_2Mn^{II}[Mn^{II}(CN)_6]$ (**3**). The genesis of this study was to identify a route to make $[NEt_4]_2[Mn^{II}(CN)_4]$,[18] as well as to prepare $[NEt_4]_4[Mn^{II}(CN)_6]$, and these results will be reported later.[19]

Experimental Section

KCN, $Mn(O_2CMe)_2\cdot 4H_2O$, and $MnCl_2\cdot 4H_2O$ were used as purchased. $Mn(O_2CMe)_2\cdot 4H_2O$ was dehydrated by heating in a vacuum oven at 100 °C over P_2O_5 for 24 h, and after putting $Mn(O_2CMe)_2\cdot xH_2O$ into the DryBox, x was determined to be 2 from a thermogravimetric analysis (TGA). RbCN was obtained as a gift from M. C. DeLong, and used as received.[20] $K_4[Mn(CN)_6]$[21a] and CsCN[21b] were prepared via literature routes. Diethyl ether was purified through an activated alumina dual-column purification system under a positive pressure of N_2, while H_2O was purified through a Barnstead "E-pure" water purification system and deoxygenated through distillation under N_2. All other solvents were distilled from the appropriate drying agents under nitrogen before use. All syntheses were performed in an oxygen-free (<1.0 ppm O_2) wet or drybox.

Physical Methods. Infrared spectra were recorded from 400 to 4000 cm^{-1} on a Bruker Tensor 37 spectrometer (±1 cm^{-1}) as KBr pellets. Thermogravimetric analyses were performed at a scan rate of 5 °C/min using a TGA 2050 TA Instruments located in a Vacuum Atmospheres DriLab under nitrogen to protect air- and moisture-sensitive samples. Samples were placed in an aluminum pan and heated at 5 °C/min under a continuous 10 mL/min nitrogen flow. Elemental analyses were performed by GCL & Chemisar Laboratories.

Magnetic susceptibilities were measured in 1000 (**1a**−**d** and **2**) and 500 Oe (**1e** and **3**) applied fields between 5 and 300 K on a Quantum Design MPMS superconducting quantum interference device (SQUID) equipped with a reciprocating sample measurement system, low field option, and continuous low temperature control with enhanced thermometry features, as previously described.[22] Powder samples for magnetic measurements were loaded in gelatin capsules. The direct current (DC) magnetization temperature dependence was obtained by cooling in zero-field and collecting the data on warming. The remanent magnetization was taken in zero applied field upon warming after cooling in a 5 Oe field. Alternating current (AC) susceptibilities were measured at 10, 100, and 1000 Hz. In addition to correcting for the diamagnetic contribution from the sample holder, the core diamagnetic corrections of −136 (**1**), −146 (**2**), and -176×10^{-6} emu/mol (**3**) were used.

Powder X-ray diffraction (XRPD) measurements for Rietveld structure analysis were performed at Beamline X16C of the National Synchrotron Light Source at Brookhaven National Laboratory. The powdered samples were held in a 1.0 mm diameter thin-wall quartz capillary. X-rays of wavelength 0.70025(1), 0.69731(1), and 0.70051(2) Å were selected by a Si(111) channel cut for $K_2Mn[Mn(CN)_6]$, $Rb_2Mn[Mn(CN)_6]$, and $Cs_2Mn[Mn(CN)_6]$, respectively. Diffracted X-rays were selected by a Ge(111) analyzer and detected by a scintillation counter. The incident intensity was monitored by an ion chamber and used to normalize the measured signal. The TOPAS-Academic program was used to index, solve, and refine the crystal structures.[23−25] Additional XRPD patterns were collected on all samples with a Bruker D8 Diffractometer (Cu Kα) using Mica (NIST Standard Reference Material 675) as an internal standard.

$K_2Mn^{II}[Mn^{II}(CN)_6]$. Method A (1a).[11] To a ∼2 mL aqueous solution of $MnCl_2\cdot 4H_2O$ (100 mg, 0.505 mmol) was added a ∼2 mL aqueous solution of KCN (100 mg, 1.54 mmol). A gray precipitate immediately formed turning yellow then green within 5 min. After 3 h of stirring, the green powder was collected by filtration, washed with water, ethanol, acetone, and diethyl ether, and dried under vacuum at room temperature for 12 h (Yield: 70 mg, 80%). IR (KBr), υ_{OH} 3628 (m), υ_{CN} 2057 (s), 2023 (sh) cm^{-1}. Calcd for $C_6K_2Mn_2N_6$: C, 20.94; H, 0.00; N, 24.42; obs C, 20.61; H, <0.20; N, 24.30.

(8) (a) Entley, W. R.; Girolami, S. G. *Inorg. Chem.* **1994**, *33*, 5165. (b) Entley, W. R.; Girolami, S. G. *Inorg. Chem.* **1995**, *34*, 2262.
(9) Franz, P.; Ambrus, C.; Hauser, A.; Chernyshov, D.; Hostettler, M.; Hauser, J.; Keller, L.; Krämer, K.; Stoeckli-Evans, H.; Pattison, P.; Bürgi, H.-B.; Decurtins, S. *J. Am. Chem. Soc.* **2004**, *126*, 16472.
(10) Klenze, R.; Kanellakopoulos, B.; Trageser, G.; Eysel, H. H. *J. Chem. Phys.* **1980**, *72*, 5819.
(11) Qureshi, A. M.; Sharpe, A. G. *J. Inorg. Nucl. Chem.* **1968**, *30*, 2269.
(12) Dong, W.; Zhu, L.-N.; Song, H.-B.; Liao, D.-Z.; Jiang, Z.-H.; Yan, S.-P.; Cheng, P.; Gao, S. *Inorg. Chem.* **2004**, *43*, 2465.
(13) Buschmann, W. E.; Ensling, J.; Gütlich, P.; Miller, J. S. *Chem.—Eur. J.* **1999**, *5*, 3019.
(14) (a) Keggin, J. F.; Miles, F. D. *Nature* **1936**, *137*, 577. (b) Itaya, K.; Uchida, I.; Neff, V. D. *Acc. Chem. Res.* **1986**, *19*, 162.
(15) Beall, G. W.; Milligan, W. O.; Korp, J.; Bernal, I. *Inorg. Chem.* **1977**, *16*, 2715. Mullica, D. F.; Zielke, J. T.; Sappenfield, E. L. *J. Sol. State. Chem.* **1994**, *112*, 92.
(16) Herren, F.; Fisher, P.; Ludi, A.; Hälg, W. *Inorg. Chem.* **1980**, *19*, 956.
(17) Kotani, M. *J. Phys. Soc. Jpn.* **1949**, *4*, 293.
(18) Buschmann, W. E.; Arif, A. M.; Miller, J. S. *Angew. Chem., Int. Ed.* **1998**, *37*, 781. *Angew. Chem.* **1998**, *110*, 813.
(19) Her, J.-H.; Stephens. P. W.; Kareis, C. M.; Moore, J. G.; Min, K. S.; Park, J.-W.; Miller, J. S., in preparation.
(20) DeLong, M. C.; Rosenberger, F. *J. Cryst. Growth* **1986**, *75*, 164.
(21) (a) Figgis, B. N. *Trans. Faraday Soc.* **1964**, *57*, 298. (b) Markley, T. J.; Toby, B. H.; Pearlstein, R. M.; Ramprasad, D. *Inorg. Chem.* **1997**, *36*, 3376.
(22) Brandon, E. J.; Rittenberg, D. K.; Arif, A. M.; Miller, J. S. *Inorg. Chem.* **1998**, *37*, 3376.
(23) *TOPAS V3: General profile and structure analysis software for powder diffraction data. - User's Manual*; Bruker AXS: Karlsruhe, Germany, 2005.
(24) Coelho, A. A. *J. Appl. Crystallogr.* **2000**, *33*, 899.
(25) TOPAS-Academic is available at http://pws.prserv.net/Alan.Coelho.

Method B (1b). To a ~2 mL, colorless aqueous solution of $Mn(O_2CMe)_2 \cdot 4H_2O$ (100 mg, 0.408 mmol) was added a ~2 mL aqueous solution of KCN (80 mg, 1.22 mmol). The color change of the precipitate was the same as observed for **1a**. The slurry was stirred for 2 h, and the green powder was collected by filtration, washed with water, ethanol, acetone, and diethyl ether, and dried under vacuum at room temperature for 12 h (Yield: 48 mg, 69%). IR (KBr), υ_{OH} 3628 (m), υ_{CN} 2057 (s), 2023 (sh) cm^{-1}. Calcd for $C_6K_2Mn_2N_6$: C, 20.94; H, 0.00; N, 24.42; obs C, 20.79; H, <0.20; N, 23.96.

Method C (1c). To a 5 mL, colorless aqueous solution of $MnCl_2 \cdot 4H_2O$ (250 mg, 1.26 mmol) was added a 5 mL aqueous solution of KCN (418 mg, 6.42 mmol). The color change of the precipitate was the same as observed for **1a**. After stirring for 3 h, the green powder was collected by filtration and washed with 2 × 10 mL water and 2 × 10 mL diethyl ether, and dried under vacuum at room temperature for 3 h (Yield: 211 mg, 97%). IR (KBr), υ_{CN} 2057 (s), 2023 (sh) cm^{-1}.

Method D (1d). To a 5 mL, colorless aqueous solution of $Mn(O_2CMe)_2 \cdot 2H_2O$ (250 mg, 1.20 mmol) was added a 5 mL aqueous solution of KCN (389 mg, 5.97 mmol). The change in color of the precipitate is the same as observed for **1a**. After stirring for 3 h, the product was collected by filtration and washed with 2 × 10 mL water and 2 × 10 mL diethyl ether, and dried under vacuum at room temperature for 3 h (Yield: 199 mg, 97%). IR (KBr), υ_{CN} 2057 (s), 2023 (sh) cm^{-1}. Calcd for $C_6K_2Mn_2N_6$: C, 20.94; H, 0.00; N, 24.42; obs C, 20.79; H, <0.20; N, 23.96.

Method E (1e). A 5 mL MeOH solution of $Mn(O_2CMe)_2$ (250 mg, 1.44 mmol) was added to ~15 mL MeOH solution KCN (329 mg, 5.05 mmol). The color change of the precipitate was the same as observed for **1a**. After stirring for 3 h, the green solid was collected by filtration, washed with 3 × 10 mL MeOH, and dried under vacuum for 2 h (yield: 160 mg, 65%). IR (KBr), υ_{CN} 2059 (s), 2023 (m) cm^{-1}. Calcd for $C_6K_2Mn_2N_6$: C, 20.94; H, 0.00; N, 24.42; obs C, 20.61; H, <0.20; N, 23.83.

$Rb_2Mn^{II}[Mn^{II}(CN)_6]$ (2). To a 5 mL aqueous solution of $Mn(OAc)_2 \cdot 2H_2O$ (172 mg, 0.701 mmol) was added a 5 mL aqueous solution containing RbCN (352 mg, 3.16 mmol). A gray precipitate immediately formed, and turned green within 5 min, and the mixture was stirred for an additional 2 h. The green powder was collected by filtration and washed with 3 × 10 mL of water, and 3 × 10 mL of diethyl ether, and dried under vacuum over P_2O_5 for 12 h (Yield: 163 mg, 90%). IR (KBr), υ_{CN} 2064 (s) and 2028 (m) cm^{-1}. Calcd for $C_6Mn_2N_6Rb_2$: C, 16.49; H, 0.00; N, 19.23; obs C, 16.34; H, <0.10; N, 18.89.

$Cs_2Mn^{II}[Mn^{II}(CN)_6]$ (3). To a 7 mL aqueous solution of $MnCl_2 \cdot 4H_2O$ (112 mg, 0.566 mmol) was added a 7 mL aqueous solution of CsCN (270 mg, 1.699 mmol). A precipitate immediately formed that turned blue-green within 1 h, and was collected by filtration and washed with water and ethanol. The solid was dried under vacuum over P_2O_5 at room temperature for 1 h (Yield: 145 mg, 96%). IR (KBr), υ_{CN} 2073 (s) cm^{-1}. Calcd for $C_6Cs_2Mn_2N_6$: C, 13.55; H, 0.00; N, 15.80; obs C, 13.14; H, <0.20; N, 15.24.

Results and Discussion

The aqueous preparation of $K_2Mn[Mn(CN)_6]$ from KCN and $MnCl_2 \cdot 4H_2O$ (**1a**), or with $Mn(OAc)_2 \cdot 4H_2O$ in a ~3:1 ratio (**1b**), exhibits a sharp υ_{OH} absorption at 3628 cm^{-1} in the IR spectra (Figure 1) that is characteristic of free (nonhydrogen bonded) water or hydroxide.[15,26] The two previous studies of $K_2Mn[Mn(CN)_6]$ did not report this

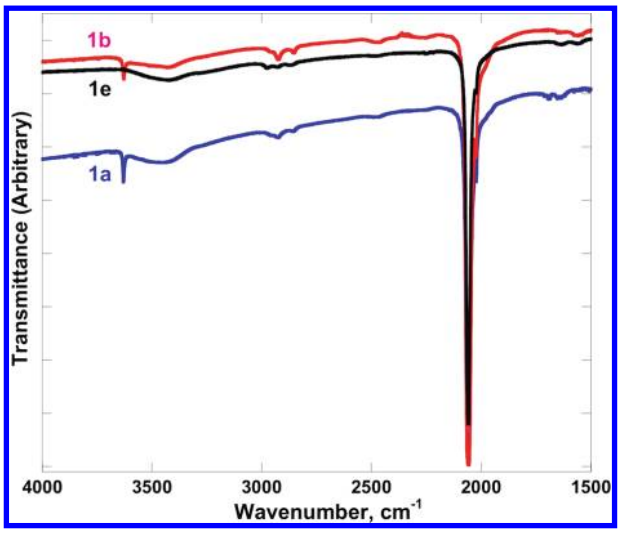

Figure 1. υ_{OH} and υ_{CN} IR spectra of **1a** (blue), **1b**–**d** (red), and **1e** (black).

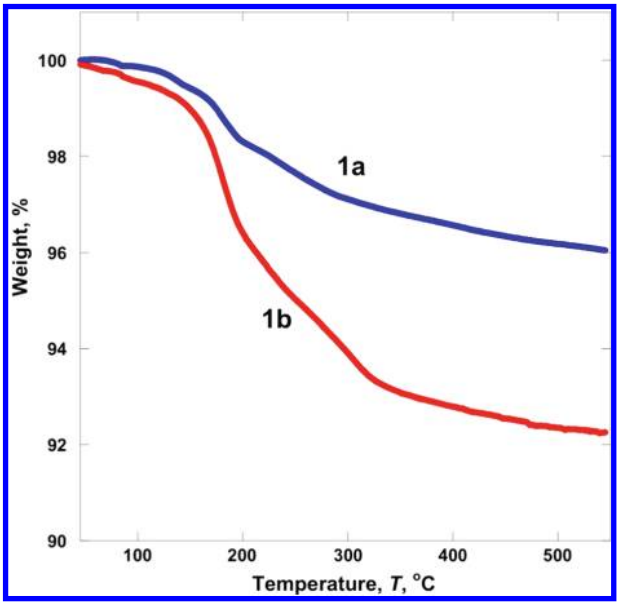

Figure 2. TGA traces for **1a** (blue) and **1b** (red).

peak.[8,11] When the reaction was carried out with an excess of KCN in water with $MnCl_2$ (**1c**) or with $Mn(OAc)_2$ (**1d**) in a ~5:1 ratio this absorption was minimal. In contrast, when prepared with $Mn(OAc)_2$ in methanol (~3:1) (**1e**), this absorption does not appear. Use of D_2O in the preparation of **1b**, or addition of D_2O to solid **1a**, leads to the shifting of this absorption to 2677 cm^{-1}, as expected for deuterium substitution; thus, this peak is assigned to water. Also, the weak absorption at 1675 cm^{-1} for **1a**, taken as a Nujol mull, is assigned as an OH bending mode. Hence, surface hydration occurs for samples prepared in water.

1a to **1e** have identical υ_{CN} IR stretching bands [and X-ray powder diffraction patterns (vide infra)]. The υ_{CN} absorption and shoulder of $K_2Mn[Mn(CN)_6]$ (**1a**–**e**) occur at 2058 and 2023 cm^{-1} (Figure 1) and occur at 2064 and 2028 cm^{-1} for $Rb_2Mn[Mn(CN)_6]$ (**2**). These are consistent with the υ_{CN} of $[Mn^{II}(CN)_6]^{4-}$ in PBAs (<2100 cm^{-1}).[6–8] The former value is in accord with 2055 ± 4 cm^{-1} previously reported for $K_2Mn[Mn(CN)_6]$.[8,11] These frequencies are lower than those

(26) Nakamoto, K. *Infrared and Raman Spectra of Inorganic and Coordination Compounds*,5th ed.; John Wiley and Sons: New York, 1997; Part A, p 161, also Part B, pp 53–57. Hornick, C.; Rabu, P.; Drillon, M. *Polyhedron* **2000**, *19*, 259.

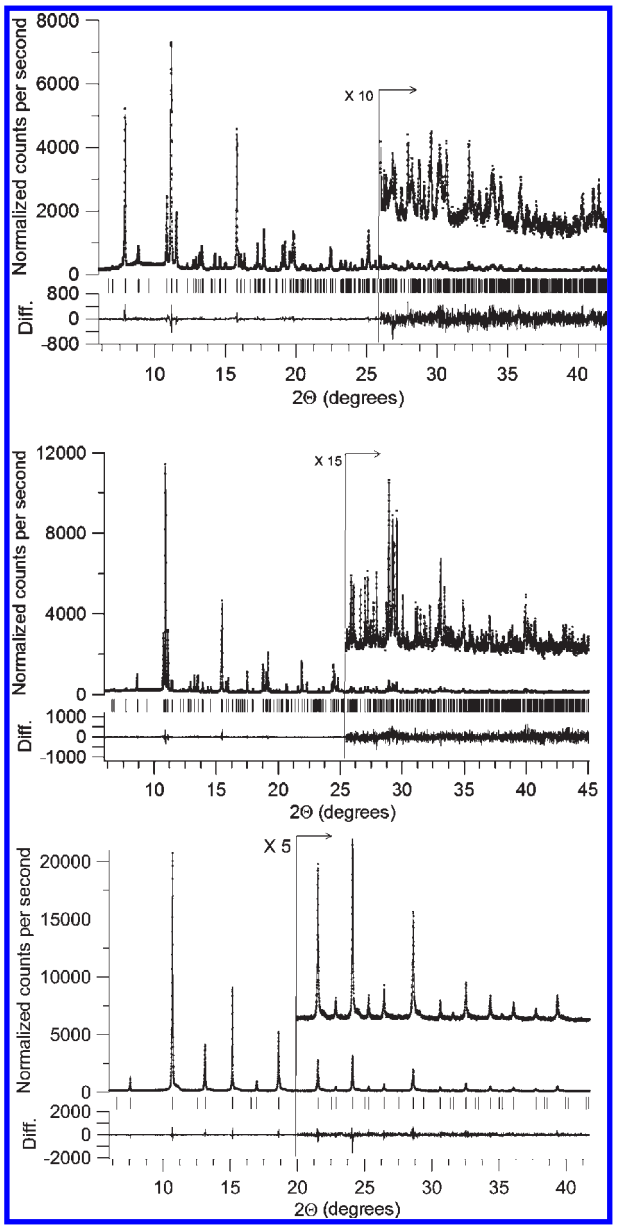

Figure 3. High-resolution synchrotron powder diffraction data (dots) and Rietveld fit (line) of the data for $K_2Mn^{II}[Mn^{II}(CN)_6]$, **1a** (top), $Rb_2Mn^{II}[Mn^{II}(CN)_6]$, **2** (middle), and $Cs_2Mn^{II}[Mn^{II}(CN)_6]$, **3** (bottom). The lower traces for each plot are the differences, measured − calculated, plotted to the same vertical scale.

of trivalent {e.g., $Mn^{III}[Mn^{III}(CN)_6]$ (2138 cm^{-1})} and tetravalent hexacyanomanganate {e.g., $M^{II}[Mn^{IV}(CN)_6]\cdot 1.4H_2O$ (2183 cm^{-1})} Prussian blue type materials,[7] because of the lower oxidation state of manganese ion. In contrast, hexacyanometalates with only M coordinated to the cyanide carbon atom have absorptions shifted to lower frequency by 20 to ~75 cm^{-1} with respect to when both the C and N bond to metal ions, as occurs for Prussian blue-type hexacyanometalates[6,27] {i.e., 2037 cm^{-1} in $K_4[Mn(CN)_6]\cdot 3H_2O$[28] vs 2058 cm^{-1} in $K_2Mn[Mn(CN)_6]$}. The two peaks are attributed to the asymmetric υ_{CN} stretching modes arising from a

Table 1. Summary of Crystallographic Parameters for $K_2Mn^{II}[Mn^{II}(CN)_6]$, **1a**, $Rb_2Mn^{II}[Mn^{II}(CN)_6]$, **2**, and $Cs_2Mn^{II}[Mn^{II}(CN)_6]$, **3**

	$K_2Mn^{II}[Mn^{II}(CN)_6]$, **1a**	$Rb_2Mn^{II}[Mn^{II}(CN)_6]$, **2**	$Cs_2Mn^{II}[Mn^{II}(CN)_6]$, **3**
MW, g/mol	344.2	436.92	531.8
a, Å	10.1786(1)	10.4102(1)	10.6061(1)
b, Å	7.4124(1)	7.4492(1)	10.6061(1)
c, Å	6.9758(1)	7.2132(1)	10.6061(1)
β, deg	90.206(1)	90.072(1)	90
V, Å^3	526.30(1)	559.36(1)	1193.06(4)
Z	2	2	4
space group	$P2_1/n$	$P2_1/n$	$Fm\bar{3}m$
ρ_{calc}, g/cm^3	2.9612(1)	2.5941(1)	2.1719(1)
R_{wp} [a,b]	0.060	0.054	0.079
R_{exp} [b,c]	0.046	0.048	0.071
T, K	293	293	293
GOF (R_{wp}/R_{exp})	1.309	1.145	1.117

[a] $R_{wp} = \{[\sum_i w_i(y_i^{calc} - y_i^{obs})^2]/[\sum_i w_i(y_i^{obs})^2]\}^{1/2}$. [b] y_i^{calc} and y_i^{obs} are the calculated and observed intensities at the *i*th point in the profile, normalized to monitor intensity. The weight w_i is $1/\sigma^2$ from the counting statistics, with the same normalization factor. *N* is the number of points in the measured profile minus number of parameters. [c] $R_{exp} = \{N/[\sum_i w_i(y_i^{obs})^2]\}^{1/2}$.

symmetry-breaking Jahn−Teller distortion for the low spin Mn^{II} ion consistent with the observed low-symmetry structure. Furthermore, absorptions at 2138, 2121, or 2097 cm^{-1} characteristic of $Mn^{III}[Mn^{III}(CN)_6]$,[7] $K_3[Mn^{III}(CN)_6]$,[29a] or $[NBu_4]_3[Mn^{III}(CN)_6]$[29b] are not observed. Evidence for the oxidative hydrolysis to Mn_3O_4[30] was also not observed.

$Cs_2Mn^{II}[Mn^{II}(CN)_6]$ (**3**) has been prepared for the first time and has a υ_{CN} absorption at 2073 cm^{-1}, but does not have any absorptions assignable to υ_{OH}. The bridged υ_{CN} absorption in **3** is ~15 cm^{-1} higher in frequency than those observed for **1**. This indicates that Mn−C bonding in **3** is weaker than in **1**. The presence of one υ_{CN} absorption indicates O_h symmetry, and is expected for a Prussian-blue structured material (vide infra).

Thermal Properties. The TGA traces for both **1a** and **1b** (Figure 2) show the weight loss to be $<0.25\%$ upon heating up to 150 °C, and 6 ± 2% weight loss upon heating up to 500 °C. The former value sets the upper limit of $0.05H_2O$ per formula. This small amount of the water implies the absence of water in the lattice. This is in accord with the observation that the intensity of the υ_{OH} peaks in **1a** and **1b** is attenuated upon heating to 70 °C for 14 h, but without a change in cell parameters, as evidenced from the XRPD pattern. The 6% weight loss below 500 °C indicates that $K_2Mn[Mn(CN)_6]$ is relatively thermally stable lattice because of the interaction of cyanide with the K^+. In contrast, $Fe[Mn(CN)_6]$ loses all of its cyanides below 500 °C.[13] Furthermore, $M[Mn(CN)_6]$ (M = V, Cr, Mn, Co, Ni) decomposes below 400 °C.[7] This suggests that the K^+ in the $K_2Mn^{II}[Mn^{II}(CN)_6]$ plays an important role of its thermal stability. Compounds **1c** and **1d**, are similar to **1a**.

Structure. The structures of **1** and **2** were solved by the simulated annealing method, and refined from the synchrotron powder diffraction data (Figure 3), and the structure of **3** was refined as the expected Prussian blue

(27) (a) Shriver, D. F.; Shriver, S. A.; Anderson, S. E. *Inorg. Chem.* **1965**, *4*, 725. (b) Dunbar, K. R.; Heintz, R. A. *Prog. Inorg. Chem.* **1997**, *45*, 288. (c) Jones, L. H.; Swanson, B. I. *Acc. Chem. Res.* **1976**, *9*, 128.

(28) Sharpe, A. G. *The Chemistry of Cyano Complexes of the Transition Metals*; Academic Press: New York, 1976.

(29) (a) Gupta, M. P.; Milledge, H. J. *Acta Crystallogr.* **1974**, *B30*, 656. (b) Buschmann, W. E.; Liable-Sands, L.; Rheingold, A. L.; Miller, J. S. *Inorg. Chim. Acta* **1999**, *284*, 175.

(30) Buckelew, A.; Galán-Mascarós, J. R.; Dunbar, K. R. *Adv. Mater.* **2002**, *14*, 1646.

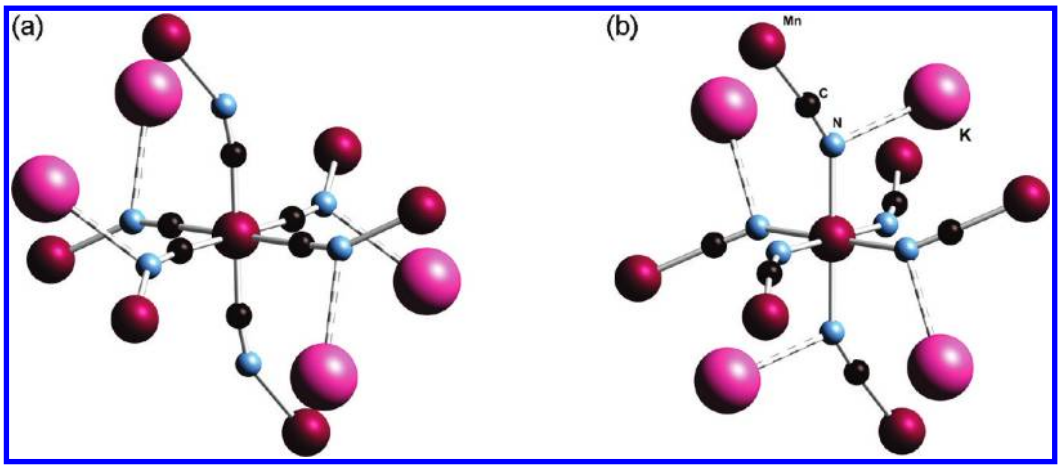

Figure 4. MnC_6 (a), and MnN_6 (b) octahedral coordination spheres for $K_2Mn^{II}[Mn^{II}(CN)_6]$, **1a**, showing the alkali$^+\cdots$N interactions (dashed lines). $Rb_2Mn^{II}[Mn^{II}(CN)_6]$, **2**, is isostructural (see TOC).

structure. At the final refinement step, all atoms were freely refined with isotropic displacement parameters (IDP). The C and N atoms of each cyano group were set to have the same IDP value. The present powder diffraction measurements do not clearly distinguish the orientation of the cyano groups; they were assigned from their bond lengths. In the $Cs_2Mn[Mn(CN)_6]$ XRPD pattern refinement, some impurity lines were observed at the higher angle tail of the major Bragg reflections, and were described as individual peaks whose centroid position, integrated intensity, and full width at half maximum were freely varied in the Rietveld process. Therefore, the structural model of $Cs_2Mn[Mn(CN)_6]$ was affected only by the sharp Bragg reflections. The crystallographic data for **1a**, **2**, and **3** are summarized in Table 1. The monoclinic unit cell of **1** differs from the cubic a = 10.15 Å previously reported for **1**;[8] hence, **1** is not a face-centered cubic that is typical of Prussian blue structured materials.[9,12]

$K_2Mn^{II}[Mn^{II}(CN)_6]$ (1a) and $Rb_2Mn^{II}[Mn^{II}(CN)_6]$ (2). Both $K_2Mn^{II}[Mn^{II}(CN)_6]$ (**1a**) and $Rb_2Mn^{II}[Mn^{II}(CN)_6]$ (**2**) are isostructural. The structure of **1a** is composed of six C-bound cyanides to a Mn(II) ion, and has two shorter Mn−C distances of 1.90(1) and 1.92(1) Å, and a longer distance of 2.01(1) Å, Figure 4a. This is attributed to a slight tetragonally elongated, Jahn−Teller distorted low-spin Mn^{II} by ∼0.1 Å. The other Mn(II) ion is high spin, and it bonds to 6 Ns with similar Mn−N bond lengths [2.18(1), 2.23(1), and 2.25(1) Å], Figure 4b. For comparison, the Mn^{II}−C bond distances vary between 1.91 and 1.98 Å for $Na_4[Mn(CN)_6]\cdot 10H_2O$.[31a,b] The Mn−C distances are 1.90(2), and 1.92(2) and slightly tetragonally elongated 1.97(2) Å, and the Mn−N distances are 2.22(1), 2.23(1), and 2.24(1) Å for **2**. The Mn^{II}−N bond for $NaMn[Cr(CN)_6]$ is 2.207(9) Å,[13] and that for $Mn_3[Co(CN)_6]_2\cdot 12H_2O$ is 2.184(9) Å.[31c] Hence, this is a nondistorted high-spin Mn^{II} ion. The CN bond distance (∼1.14 Å) is not sensitive to the chemical environment.[10,31d,e]

The Mn−C−N angles of 168.7(9), 172.9(7), and 178(1)° (average = 173°) for **1a**, and 176(2), 177(1), and 179(1) (average 177°) for **2** approach linearity, as expected. However, the Mn−N−C angles of 152.7(7), 148.2(7), and 145.6(7)° (average = 148.8°) for **1**, and 150(1), 153(1), and 157(1)° (average = 153.3°) for **2** deviate substantially from linearity, an unexpected result for a Prussian blue structured material.

Each cyanide bridges a low- and a high-spin Mn(II) ion to form a three-dimensional (3-D) framework structure with void spaces occupied by K^+ (**1a**, Figures 4 and 5) or Rb^+ ions (**2**). The $Mn^{II}\cdots Mn^{II}$ separations are 5.09 and 5.19 Å for **1a** and **2**, respectively, which are slightly shorter than the Mn$\cdots$Cr separations in $NaMn[Cr(CN)_6]$ (5.41 Å)[12] [and 5.30 Å for $Cs_2Mn[Mn(CN)_6]$ (vide infra)] that also possesses nonlinear M−N−C bonding. As a consequence, MnC_6, and MnN_6 occur in alternating rows and have their octahedra tilting in opposing directions (Figure 5). The K^+ and Rb^+ ions interact with seven cyanide nitrogens with $K^+\cdots N$ and $Rb^+\cdots N$ distances that range from 2.98 to 3.50 Å, and 3.15 and 3.59 Å for **1** and **2**, respectively. The alkali ion interactions with the cyanide ligands occurs in all directions, and leads to a 3-D zigzag network of the Mn−CN−Mn bonds. Due to the observation of the ν_{OH} absorption for **1a**, crystallographic evidence was sought, but could not be identified, in the Fourier difference map, and is in accord with the presence of surface water.

In contrast to a cubic Prussian blue structural motif where the void spaces are defined by the cubic framework arrangement of atoms arising from covalent M−CN and M′−NC bonding leading to linear M−CN−M′ angles, the less covalent Mn^{II} (more ionic)[32] can accommodate a reduced M−CN−M′ angle induced from the electrostatic interactions increase with decreasing cation size ($K^+ > Rb^+ > Cs^+$) minimizing void space, as occurs. Similar, bent cyanide bridged ligands with nonlinear Mn−N−C angles of 152.7 and 153.4° have been observed for $A[(Me_3tacn)_6MnCr_6(CN)_{18}](ClO_4)_3$ (A = Na, K; Me_3tacn = *N*,*N*′,*N*″-trimethyl-1,4,7-triazacyclononane)

(31) (a) Tullberg, A.; Vannerberg, N. *Acta Chem. Scand. A* **1974**, *28*, 551. (b) Tullberg, A.; Vannerberg, N.-G. *Acta Chem. Scand.* **1971**, *25*, 343. (c) Beall, G. W.; Milligan, W. O.; Korp, J.; Bernal, I. *Inorg. Chem.* **1977**, *16*, 2715. (d) Brown, D. B.; Shriver, D. F. *Inorg. Chem.* **1969**, *8*, 37. (e) Ludi, A.; Güdel, H. U. *Struct. Bonding* (*Berlin*) **1973**, *14*, 1.

(32) Covalency increases with crystal field stabilization, Δ_o; hence, high spin $Mn^{II}-N_6$ is more ionic than low spin $Mn^{II}-C_6$.Mingos, D. M. P. *Essential Trends in Inorganic Chemistry*; Oxford University Press: New York, 1998; p 331.

(33) (a) Heinrich, J. L.; Sokol, J. J.; Hee, A. G.; Long, J. R. *J. Sol. State Chem.* **2001**, *159*, 293. (b) Rodríquez-Hernández, J.; Reguera, E.; Lima, E.; Balmaseda, J.; Martínez-Garcia, R.; Yee-Maderia, H. *J. Phys. Chem. Sol.* **2007**, *68*, 1630. (c) Escorihuela, I.; Falvello, L. R.; Tomás, M. *Inorg. Chem.* **2001**, *40*, 636.

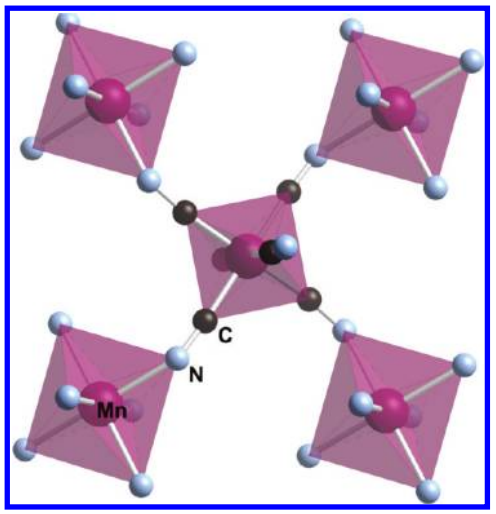

Figure 5. View normal to the *bc* plane of the 3-D network lattice for $K_2Mn^{II}[Mn^{II}(CN)_6]$, **1a**, showing MnC_6 surrounded by four MnN_6 octahedra pointing in different directions (K^+ are not shown for clarity). $Rb_2Mn^{II}[Mn^{II}(CN)_6]$, **2**, is isostructural.

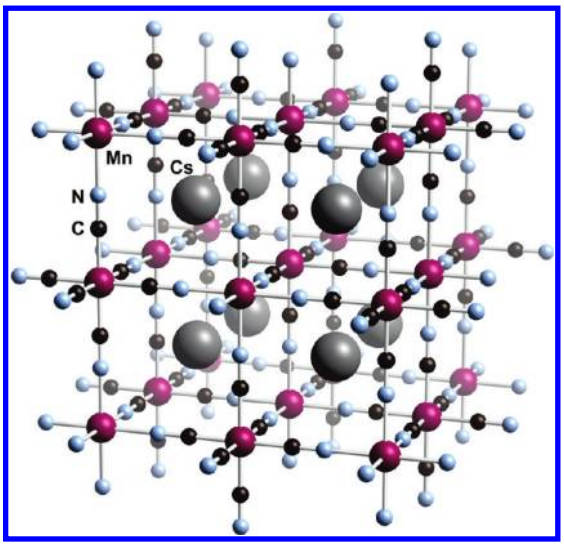

Figure 6. Structure of $Cs_2Mn^{II}[Mn^{II}(CN)_6]$, **3**, showing the usual fcc Prussian blue structure.

also possessing high spin Mn^{II}.[33a] Likewise, Zn−N−C angles ranging from 151.4 and 165.1° have been reported for $Zn_3[M^{III}(CN)_6]_2$ (M = Fe, Co), $Zn_3A_2[Fe^{II}(CN)_6]_2$ ($A = Rb^+$, NH_4^+) possessing ionic Zn^{II},[33b] and an even further reduced Cu^{II}−N−C angle of 120.1° has been documented.[33c]

$Cs_2Mn^{II}[Mn^{II}(CN)_6]$ (3). $Cs_2Mn^{II}[Mn^{II}(CN)_6]$ (**3**) exhibits the typical cubic Prussian Blue structure[34] [a = 10.6061(1) Å] with one hexacoordinate Mn(II) surrounded by six 6 C-bound cyanides, and the other Mn(II) surrounded by six 6 N-bound cyanides, with linear MnCNMn linkages. The Mn−C, Mn−N, and C−N distances are 1.93(1), 2.19(1), and 1.18(1) Å, respectively, Figure 6. Hence, structural evidence for Jahn−Teller distortion about the low spin Mn(II) site is not present. The Mn(II)···Mn(II) separation is $a/2$ (5.303 Å). The cubic unit cell is very similar to that of $NaMn[Cr(CN)_6]$ [a = 10.8159(12) Å].[12] Hence, **3** has a structure that is typical of Prussian blue.

Comparison of the $A_2Mn^{II}[Mn^{II}(CN)_6]$ (A = K, Rb, Cs) Structures. The $A_2Mn^{II}[Mn^{II}(CN)_6]$ (A = K, Rb) structural motif is unusual and differs from the well-known fcc Prussian blue motif[31e] as a consequence of its monoclinic unit cell. Perspective views of the Prussian blue and $Rb_2Mn^{II}[Mn^{II}(CN)_6]$ structures are shown in Figure 7. The new motif is related to the Prussian blue lattice parameters that are approximately a, $a/\sqrt{2}$, $a/\sqrt{2}$, $\beta \sim 90°$. The distortion from an orthorhombic lattice is small, but it is clearly required by the raw data, as shown by profile fits in the Supporting Information, Figures S3 and S4. The nonlinear Mn−C−N−Mn linkages for the latter lead to canting of the octahedra, as described above (Figure 5), and buckling of the 3-D lattice, Figure 7. This is also observed looking down the a-axis, Figure 8. For both structure types 3-D channels are present that are filled by the alkali cations, Figure 8.

(34) The observed XRPD pattern of **3** can also be equally well-explained with the $Fm\bar{3}c$ space group symmetry whereby all C and N are positionally disordered, but this was discarded, as it is inconsistent with the structure of the other PBAs, and the magnetic data.

Magnetic Properties. The magnetic susceptibilities, $\chi(T)$, of **1**−**3** as well as $K_4[Mn(CN)_6]\cdot 3H_2O$ were measured between 5 to 300 K, and are plotted as $\chi T(T)$, Figures 9 and 10, and the results are summarized in Table 2. [See Supporting Information, Figures S1 and S2 for the $\chi(T)$ data.] $K_4[Mn(CN)_6]$ has a room temperature χT value of 0.50 emu K/mol that exceeds the low-spin spin-only value 0.375 emu K/mol for Mn^{II} indicative of an orbital contribution and g = 2.31. The χT value decreases slightly with decreasing temperature to 0.45 emu K/mol at 60 K, followed by a big decrease to 0.275 emu K/mol at 2 K, indicating either an intermolecular interaction or a spin−orbit interaction (λ). For $K_4[Mn(CN)_6]$, it is known that the magnetic moment has a range of 0.48 to 0.59 emu K/mol,[17] and attempts to obtain the spin−orbit interaction (λ) for $K_4[Mn(CN)_6]$[17] were unsuccessful because of the large deviation below ~100 K.

$K_2Mn^{II}[Mn^{II}(CN)_6]$ (1). 1a and **1e** have room-temperature χT values of 5.56 and 5.10 emu K/mol, respectively, and like the previously reported values of 4.99[8] and 5.13[11] emu K/mol for $K_2Mn[Mn(CN)_6]$ exceed the 4.75 emu K/mol expected for the spin-only value for one low- and one high-spin Mn(II) site. This is indicative of an anisotropic orbital contribution from the low spin Mn(II), and the differing average orientations of the polycrystalline samples. These values decrease upon cooling and reach shallow minima of 4.99 and 5.11 emu K/mol at 90 and 105 K, respectively, and then increase and reach maxima of 100 ± 2 emu K/mol at 32 ± 1 K for **1a** and **1e**, Figure 10. Above 120 K, the $\chi^{-1}(T)$ can be fit to the Curie−Weiss expression, $\chi \propto (T - \theta)^{-1}$, with $\theta = -63 \pm 3$ K, indicating significant antiferromagnetic couplings. The significant increase in $\chi T(T)$ at low temperature suggests the onset of magnetic ordering. Likewise, previously $K_2Mn[Mn(CN)_6]$ was reported to reach a minimum at 105 K, and then increase and reach maxima of 1325 emu K/mol at 24 K as well as $\theta = -19$ K from data taken between 100 and 290 K.[8a]

A fit of the $\chi^{-1}(T)$ data to the Néel hyperbolic equation, eq 1 {where C and θ are the Curie and Weiss constants, respectively, and θ' and ζ are proportional to $\eta_A\eta_B C(\eta_A - \eta_B)$ and $\eta_A\eta_B C$ (where η_i is the fractional occupancy of

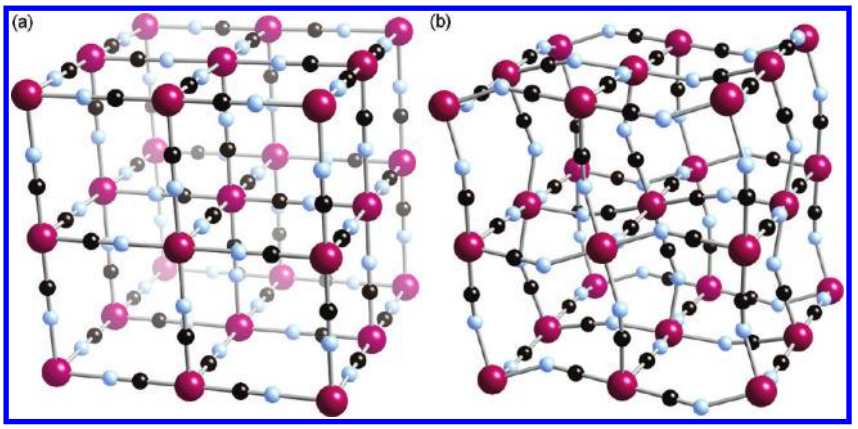

Figure 7. Perspective views of the Prussian blue structured $Cs_2Mn^{II}[Mn^{II}(CN)_6]$, **3**, (a), and non-Prussian blue structured $Rb_2Mn^{II}[Mn^{II}(CN)_6]$ (b).

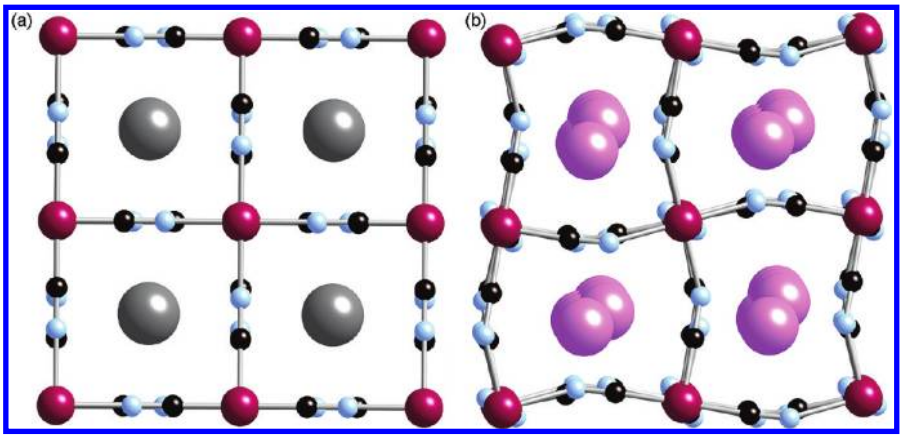

Figure 8. Views along the *a*-axis for $Cs_2Mn^{II}[Mn^{II}(CN)_6]$ (**3**) (a), and non-Prussian blue structured $Rb_2Mn^{II}[Mn^{II}(CN)_6]$ (**2**) (b) showing the location of the respective cations, and buckling of the lattice for (**2**).

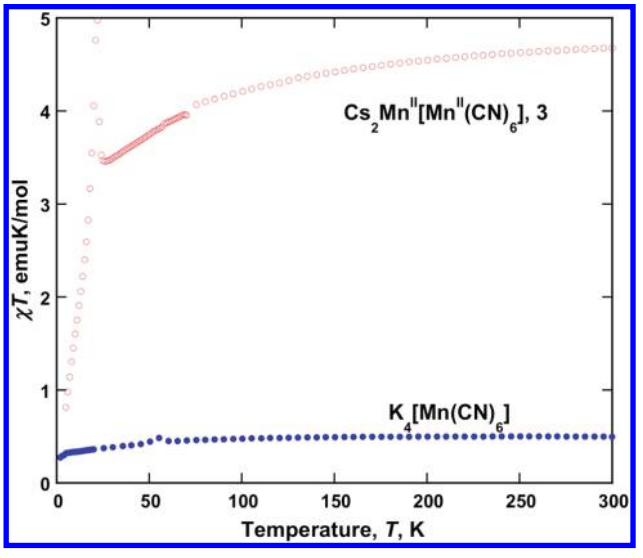

Figure 9. $\chi T(T)$ for $K_4[Mn(CN)_6]$ (solid blue circles), and Cs_2Mn^{II}-$[Mn^{II}(CN)_6]$, **3** (open red circles).

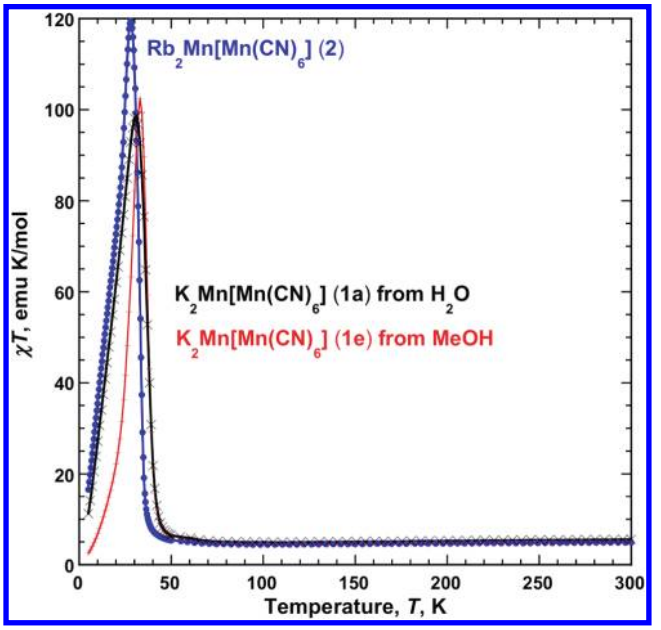

Figure 10. $\chi T(T)$ for **1a** (×), **1e** (+), and **2** (solid blue circles). The lines are guides for the eye.

each sublattice site), respectively}[35] (Figure 11) gives a T_c of 41 K for both **1a** and **1e**.

$$\chi^{-1} = \frac{T-\theta}{C} - \frac{\zeta}{T-\theta'} \quad (1)$$

The field-cooled (FC) and zero-field-cooled (ZFC) magnetizations for **1a** and **1e** were measured in a 5 Oe magnetic field (Figure 12). The bifurcation temperature, T_b, of the FC/ZFC magnetizations of 47 and 46 K for **1a** and **1e**, respectively.

The 5 K field dependence of the magnetization, $M(H)$, shows a rapid rise with increasing field, H, with respect to

Table 2. Summary of Magnetic Properties for **1**−**3**

	1a	**1e**	$K_2Mn[Mn(CN)_6]$[8]	**2**	**3**
cation	K^+	K^+	K^+	Rb^+	Cs^+
$\chi_{obs}T$, emu K/mol (295 K)	5.56	5.10	4.99,[8] 5.13[11]	4.83	4.68
$\chi_{calc}T$, emu K/mol (spin-only)	4.75	4.75	4.75	4.75	4.75
θ, K (Curie−Weiss)	−60	−65	−19	−30	−15
θ, K (Néel), eq 1	−33	−20	b	−19	−15
T_N, K (Néel), eq 1	41	41	41	34.6	21
T_b, K (ZFC/FC)	47	46	b	38	24
T_f, K (ac)	38	38	b	34	22
H_{cr}, Oe	3900	9150	370	8850	5000
M, emu Oe/mol (5 K, 50 kOe)	16,100	15,800	24,000 [a]	16,300 [c]	9360 [c]
M_r, emu Oe/mol	8600	9350	430	9300	640

[a] 4.5 K, 70 kOe.[8] [b] Not reported. [c] Not saturated. [d] 19,150 emu Oe/mol at 90 kOe.

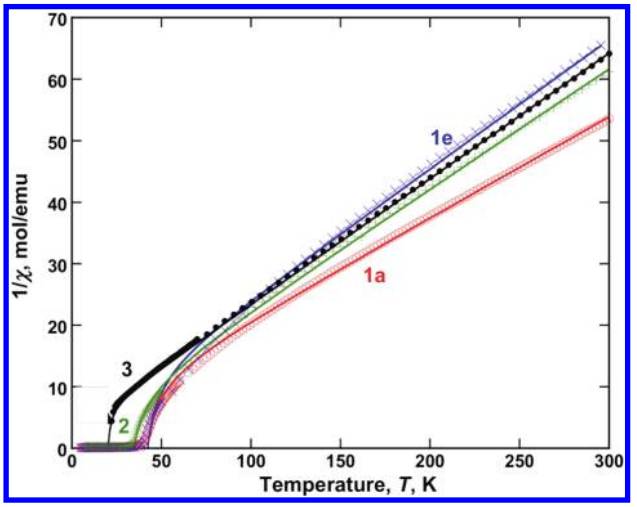

Figure 11. $\chi^{-1}(T)$ for **1a** (○, red), **1e** (×, blue), **2** (+, green), and **3** (●, black). The solid lines represent the best-fit curves to the Néel hyperbolic equation, eq 1.

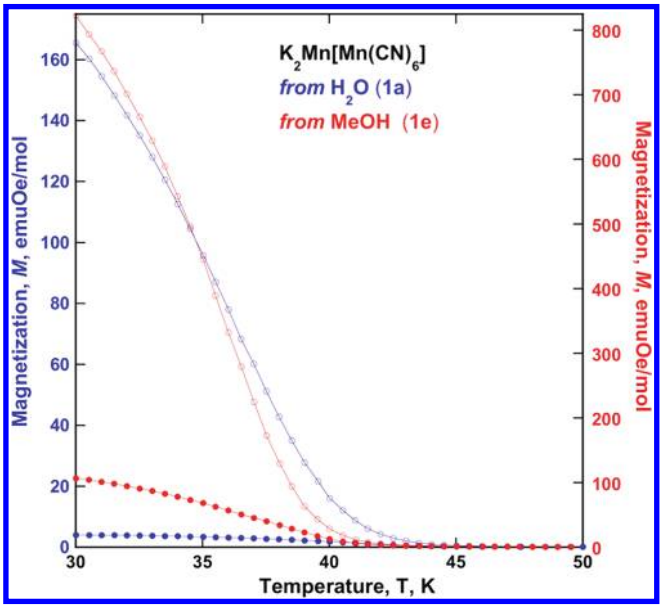

Figure 12. Field-cooled (FC, filled circles) and zero-field-cooled (ZFC, open circles) $M(T)$ for **1a** (blue), and **1e** (red) showing the bifurcation temperatures.

the expectation from the Brillouin expression, is suggestive of magnetic ordering for **1a** and **1e** (Figure 13). The 50 kOe magnetizations at 5 K are 16, 100, and 15,800 emu Oe/mol for **1a** and **1e**, respectively, but are still gradually rising with increasing field. Hence, they are in accord with the expectation of 22,340 emu Oe/mol for antiferromagnetic coupling leading to ferrimagnetic ordering, and are consistent with the reported 70 kOe magnetization at 4.5 K that is 24,000 emu Oe/mol for $K_2Mn[Mn(CN)_6]$.[8] At 5 K the remanent magnetizations, M_r, are 8600 and 9350 emu Oe/mol, and the coercive fields, H_{cr}, are 3900 and 9150 Oe for **1a** and **1e**, respectively (Figure 13). Hence, the biggest difference between the sample that has a υ_{OH} absorption (i.e., **1a**), and the one that does not (i.e., **1e**), is the more than doubling of the H_{cr}, but in both cases they exceed the previously reported value of 370 Oe.[8]

In addition, peaks in both the frequency-independent in-phase, $\chi'(T)$, and out-of-phase, $\chi''(T)$, components of the AC susceptibility for **1a** and **1e** occur, and are characteristic of ferri- or ferromagnetic ordering, Figure 14. Using the maximum in the 10 Hz $\chi'(T)$ data, T_c = 38 K, which is a bit reduced from the bifurcation temperature, T_b.

The 41 K T_c for $K_2Mn[Mn(CN)_6$ is in contrast to that of the isoelectronic $Fe^{III}[Fe^{III}(CN)_6]\cdot 4H_2O$ with low spin Fe^{III} (t_{2g}^5, S = 1/2) and high spin Fe^{III} ($t_{2g}^3e_g^2$, S = 5/2)

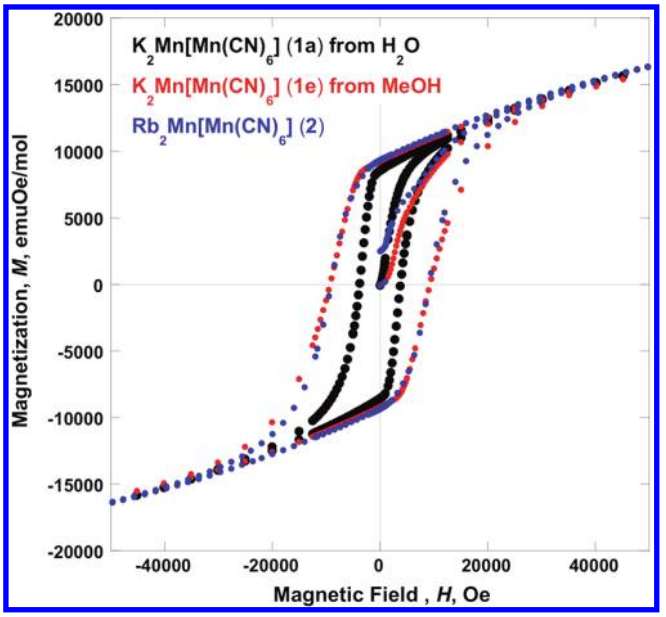

Figure 13. $M(H)$ for **1a** (black circles), **1e** (red circles), and **2** (blue circles).

(35) (a) Néel, L. *Ann. Phys.* **1948**, *3*, 137. (b) Smart, J. S. *Am. J. Phys.* **1955**, *23*, 356.

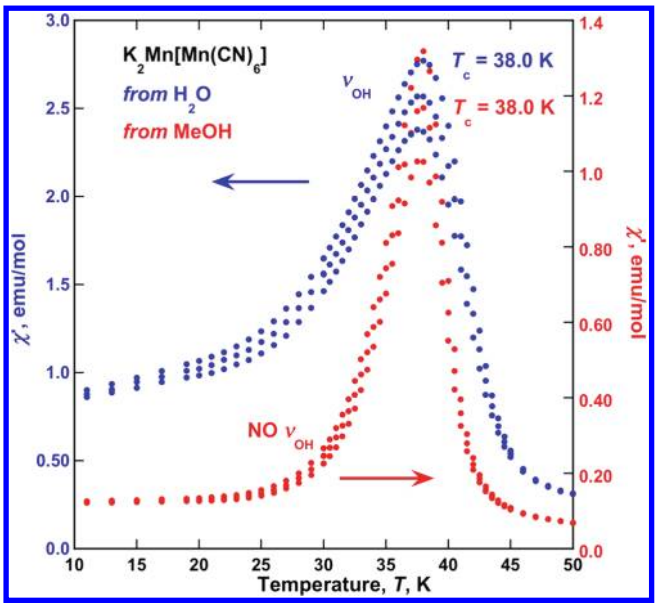

Figure 14. $\chi'(T)$ for **1a** (blue circles) and **1e** (red circles) showing the 38 K ordering temperature.

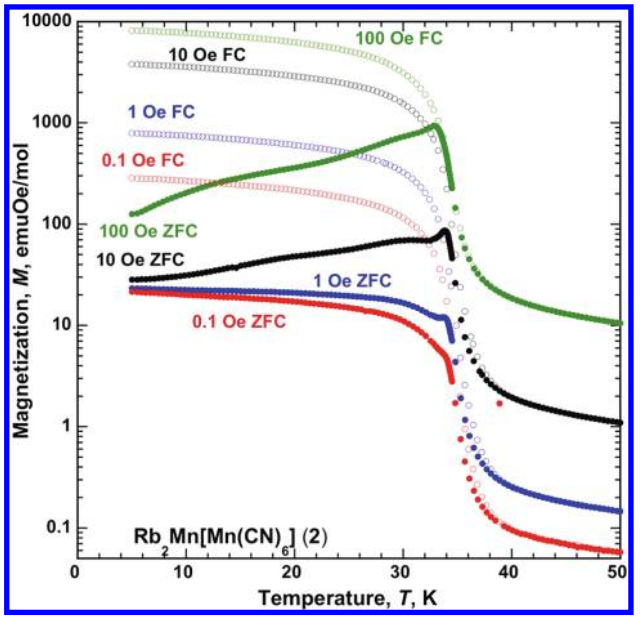

Figure 15. Field-cooled (FC) (open circles) and zero-field-cooled (ZFC) (filled circles) $M(T)$ for **2** at 0.1 (red), 1 (blue), 10 (black), and 100 Oe (green) applied fields.

that exhibits a lower T_c of 17.4 K and H_{cr} of 465 Oe.[36] $Fe^{III}[Fe^{III}(CN)_6]\cdot 4H_2O$ possesses a fcc structure with water molecules in the interstitial sites. Thus, the bent Mn−CN−Mn bond contributes to the higher magnetic ordering temperature and coercive field of $K_2Mn[Mn(CN)_6]$ with respect to $Fe^{III}[Fe^{III}(CN)_6]\cdot 4H_2O$. The $Mn^{II}\cdots Mn^{II}$ separations of 5.09 Å are identical to the $Fe^{III}\cdots Fe^{III}$ distance of 5.1090(5) Å; thus, the bent cyanide bridges, rather than the short distance between the spin centers, play a crucial role in the superexchange mechanism. The more ionic character (less directional covalency) associated with Mn^{II} with respect to Fe^{II} [32] accommodates the significantly reduced Mn−N−C angle

(36) Kumar, A.; Yusuf, S. M.; Keller, L. *Phys. Rev. B* **2005**, *71*, 054414.

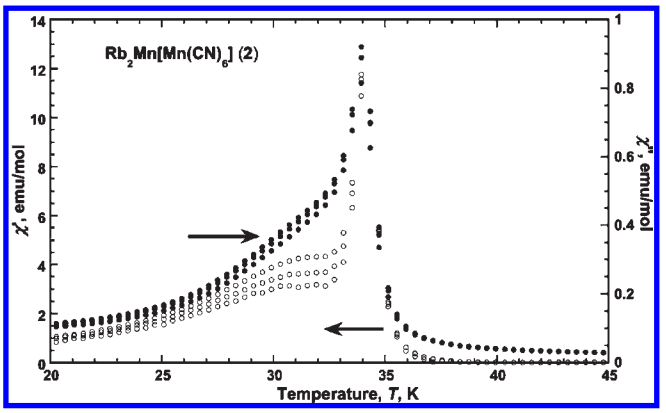

Figure 16. $\chi'(T)$ (●) and $\chi''(T)$ (○) for **2** at 10, 100, and 1000 Hz.

with respect to the Fe−N−C angle, stabilizing the observed solvent-free non-Prussian blue structure

$Rb_2Mn^{II}[Mn^{II}(CN)_6]$ (2). The room temperature χT value for **2** is 4.83 ± 0.07 emu K/mol, and is also in accord with 4.75 emu K/mol expected for the spin-only value for one low- and one high-spin Mn(II) site (Figure 8).[37] The $\chi T(T)$ decreases upon cooling and reaches a minimum of 4.40 emu K/mol at 100 K, before again increasing to 117 emu K/mol at 28 K. Above 170 K, the $\chi^{-1}(T)$ data can be fit to the Curie−Weiss expression with $\theta = -30$ K, indicating antiferromagnetic coupling, albeit weaker, than observed for **1a** and **1e**. The large increase in $\chi T(T)$ at low temperature suggests the onset of magnetic ordering. The T_c of 34.6 K was obtained from fitting the data to Néel's hyperbolic equation, eq 1 (Figure 11).[8,10] This is reduced from 41 K for $K_2Mn[Mn(CN)_6]$.

The 1 Oe FC/ZFC magnetizations for **2** exhibit a T_b of 38 K (Figure 15, $H \leq 10$ Oe). Unlike for **1a** and **1e**, the ZFC magnetizations exhibit an anomaly (bump) at ~34 K, whose intensity increases with applied field (Figure 15). This suggests a transition to a second magnetic phase upon cooling; however, the nature of this is unknown, but might arise from canting. To rule out an extrinsic impurity, an independent sample was studied, and the magnetic data were in quantitative agreement.

The 5 K $M(H)$ shows a rapid rise with increasing field, H, which with respect to the expectation from the Brillouin expression is suggestive of magnetic ordering (Figure 13). At 90 kOe the magnetization is 19,250 emu Oe/mol and still rising; hence, it is in accord with the expectation of 22,340 emu Oe/mol for antiferromagnetic coupling leading to ferrimagnetic ordering. As shown in Figure 13, **2** has a significant coercive field of 8850 Oe, remanent magnetization, M_r, of 9300 emu Oe/mol at 5 K, and the hysteresis is almost identical to that for **1e** (Figure 13).

In addition, peaks in both the frequency-independent $\chi'(T)$ and $\chi''(T)$ for **2** occur and are characteristic of ferri- or ferromagnetic ordering, Figure 16. Using the maximum in the 10 Hz $\chi'(T)$ data, $T_c = 34$ K, which is a bit reduced from the 38 K bifurcation temperature, T_b. $\chi'(T)$ has a shoulder at ~29 K and $\chi''(T)$ exhibits a second

(37) It is also substantially greater than the 1.0 emu Oe/mol expected for two low-spin, $S = 1/2$ Mn^{II} ($g \sim 2.3$) sites, and is substantially lower than the 8.75 emu Oe/mol expected for two high-spin, $S = 5/2$ Mn^{II} ($g \sim 2.0$) sites.

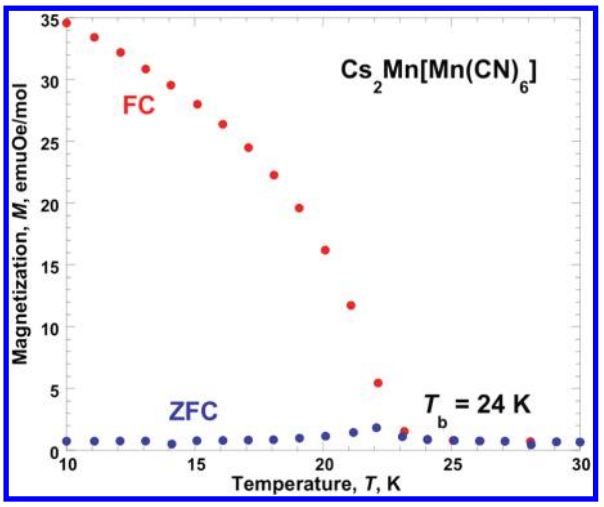

Figure 17. Field-cooled (FC) (red circles) and zero-field-cooled (ZFC) (blue circles) $M(T)$ for **3** showing the bifurcation temperature, T_b.

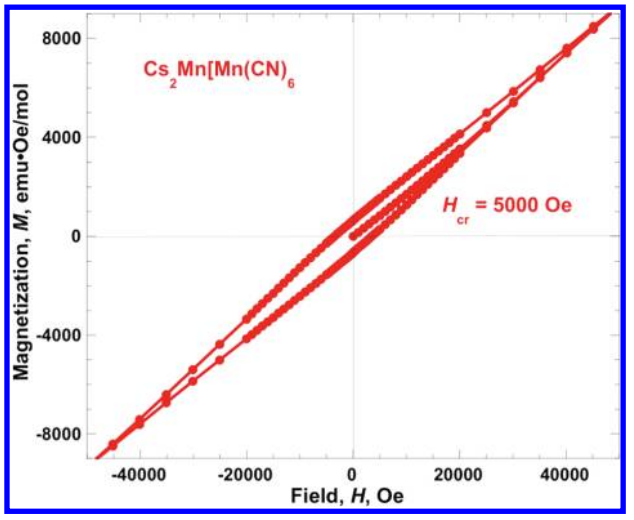

Figure 18. $M(H)$ for **3**.

absorption at ~ 30 K that are suggestive of an unknown second magnetic phase, and is also indicated from the FC/ZFC magnetization data, Figure 15.

$Cs_2Mn^{II}[Mn^{II}(CN)_6]$ (3). The room temperature χT value for **3** is 4.68 emu K/mol, and like **1a** to **1e**, is in accord with 4.75 emu K/mol expected for the spin-only value for one low- and one high-spin Mn(II) site (Figure 9).[38] $\chi T(T)$ decreases upon cooling and reaches a minimum of 3.46 emu K/mol at 26 K, before again increasing to 6.3 emu K/mol at 22 K. Above 25 K, the $\chi^{-1}(T)$ data can be fit to the Curie−Weiss expression with $\theta = -15$ K, indicating antiferromagnetic coupling, albeit weaker, than observed for **1a**, **1e**, **2**, and **3**. The increase in $\chi T(T)$ at low temperature suggests the onset of magnetic ordering.

The 5 Oe FC/ZFC magnetizations for **3** (Figure 17) exhibit a T_b of 24 K. The T_c of 21 K was obtained from fitting the data to Néel's hyperbolic equation, eq 1, (Figure 11).[8,10] This is reduced from that reported for **1a** and **1e**.

(38) It is also substantially greater than the 1.0 emu Oe/mol expected for two low-spin, $S = 1/2$ Mn^{II} ($g \sim 2.3$) sites, and is substantially lower than the 8.75 emu Oe/mol expected for two high-spin, $S = 5/2$ Mn^{II} ($g \sim 2.0$) sites.

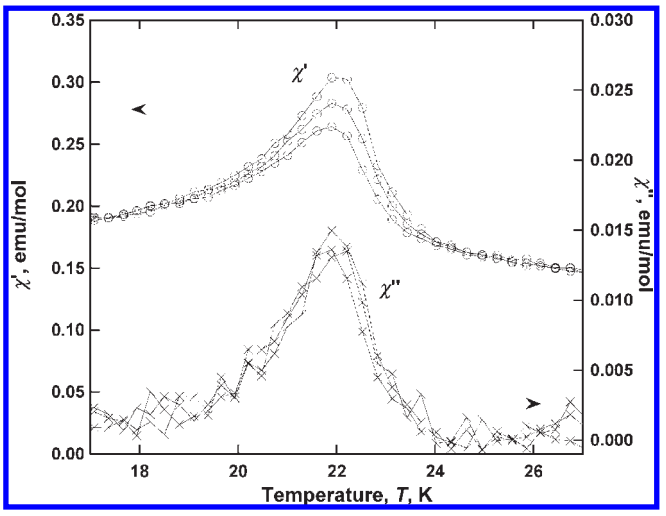

Figure 19. $\chi'(T)$ (○) and $\chi''(T)$ (×) for **3** showing the their 22 K T_c.

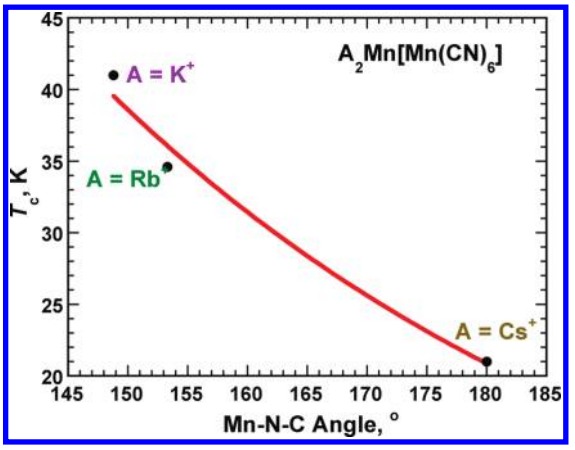

Figure 20. Correlation of increasing T_c with deviation from linearity of the Mn−N−C angle for $A_2Mn[Mn(CN)_6]$ (A = K, Rb, Cs).

The magnetization at 50 kOe is 9360 emu Oe/mol and is still rising without evidence of saturating. As shown in Figure 18, **3** has a significant coercive field of 5000 Oe and remanent magnetization of 640 emu Oe/mol at 5 K, and the shape of the hysteresis curve is quite unusual. The source of the unusual shape of the $M(H)$ curve, the high coercivity, and lack of approaching saturation is unknown.

Peaks in both $\chi'(T)$ and $\chi''(T)$ characteristic of ferri- or ferromagnetic ordering are also observed, Figure 19. Using the maximum in the 10 Hz $\chi'(T)$ data, a T_c of 22 K, that is reduced from the bifurcation temperature, T_b, is observed. The $\chi'(T)$ data of **3** has a small frequency dependence with the temperatures of each maximum being almost constant $\{\phi \sim 0;\ \phi = \Delta T_f[T_f\Delta(\log f)]^{-1};$ where T_f is the temperature of the peak in the lowest frequency (10 Hz) data; and f is the frequency in hertz$\}$ indicating no spin glass behavior. The out-of-phase, imaginary, $\chi''(T)$ data displays a peak below 24 K, indicating magnetic ordering.

Conclusion

$K_2Mn[Mn(CN)_6]$ was made in aqueous (**1a**) or non-aqueous (**1e**) media. **1a** has a sharp ν_{OH} absorption in the IR

spectrum, while **1e** does not. Use of D_2O shifts this peak as expected for deuteration. While this supports the presence of H_2O, that is not evident from the structure, TGA, XRPD, or elemental analysis; thus, it is attributed to surface water, and it may arise from surface hydrolysis. $K_2Mn[Mn(CN)_6]$ has a bent (148.8°) Mn−CN−Mn framework that is different with respect to the face-centered structures typical of PBAs. This nonlinearity is attributed to the ionic nature if high spin Mn(II) strong interactions between K^+ and cyanide ions. **1a** and **1e** exhibit essentially identical structures and similar magnetic properties. $Rb_2Mn[Mn(CN)_6]$ (**2**) is isostructural to $K_2Mn[Mn(CN)_6]$; however, the longer $Rb^+\cdots N$ distances with respect to $K^+\cdots N$ provide weaker electrostatic interactions decreasing the nonlinearity of the Mn−N−C linkages to 153.3°. This distortion from the traditional fcc Prussian blue structure is not observed for the isoelectronic $Fe^{III}[Fe^{III}(CN)_6]\cdot 4H_2O$ because of the greater charges and greater covalency (reduced ionic character).

$Cs_2Mn[Mn(CN)_6]$ has the archetypal fcc Prussian blue structure and is magnetically characterized to order as a ferrimagnet at 21 K. While saturation does not occur at 50,000 Oe, it has a remanent magnetization of 640 emu Oe/mol and a large coercive field of 5 kOe at 5 K. The latter is attributed to the positional disorder of the cyanides.

The 41 K T_c for $K_2Mn[Mn(CN)_6]$ is in contrast to isoelectronic $Fe^{III}[Fe^{III}(CN)_6]\cdot 4H_2O$ with low spin Fe^{III} (t_{2g}^5, $S = 1/2$) and high spin Fe^{III} ($t_{2g}^3e_g^2$, $S = 5/2$) that exhibits a lower T_c of 17.4 K and H_{cr} of 465 Oe.[36] The T_c is comparable to that for Prussian blue structured **3**. Furthermore, T_c increases as $K^+ > Rb^+ > Cs^+$ for $A_2Mn[Mn(CN)_6]$ (A = K, Rb, Cs) and this correlates with the increasing deviation of linearity of the Mn−N−C linkages of 31.2 (K^+) > 26.7 (Rb^+) > 0° (Cs^+), Figure 20, and decreasing Mn(II)···Mn(II) separations of 5.09 (K^+) < 5.19 (Rb^+) < 5.30 Å (Cs^+). This suggests that the bent cyanide bridges play a crucial role in the superexchange mechanism by increasing the coupling via shorter Mn(II)···Mn(II) separations, and perhaps enhanced overlap. MO calculations are needed to provide insight into this. Furthermore, use of the smaller Na^+ cation should lead to stronger interactions increasing T_c, and increasing pressure should lead to greater deviation of the MnNC angle from linearity and increase T_c.

Acknowledgment. We appreciate the sample of RbCN provided by Mathew C. DeLong (Department of Physics, University of Utah) and the helpful discussions with Profs. Larry R. Falvello (University of Zaragoza), Jeffrey Long (University of California, Berkeley), and assistance from Saul Lapidius (Department of Physics and Astronomy, Stony Brook University) and Kendric J. Nelson (Utah), and the continued partial support by the Department of Energy Division of Material Science (Grants DE-FG03-93ER45504 and DE-FG02-01ER4593). Use of the National Synchrotron Light Source, Brookhaven National Laboratory, was supported by the U.S. Department of Energy, Office of Basic Energy Sciences, under Contract No. DE-AC02-98CH10886.

Supporting Information Available: The powder X-ray crystallographic information files (CIF) for $K_2Mn^{II}[Mn^{II}(CN)_6]$, $Rb_2Mn^{II}[Mn^{II}(CN)_6]$, and $Cs_2Mn^{II}[Mn^{II}(CN)_6]$ (CCDC 709700, 723397, and 709701), $\chi(T)$ for $K_4[Mn(CN)_6]$, **1a**, **1e**, **2**, and **3**, and fits of the observed PXRD data for **1a** and **2** assuming orthorhombic and monoclinic space groups. This material is available free of charge via the Internet at http://pubs.acs.org.